Front. Earth Sci. 2018, 12(3): 545–554
https://doi.org/10.1007/s11707-017-0676-6

RESEARCH ARTICLE

In-situ stress distribution and coalbed methane reservoir permeability in the Linxing area, eastern Ordos Basin, China

Wei JU (✉)[1,2], Jian SHEN[1,2], Yong QIN[1,2], Shangzhi MENG[3], Chao LI[2], Guozhang LI[2], Guang YANG[2]

1 Key Laboratory of Coalbed Methane Resources and Reservoir Formation Process, Ministry of Education, China University of Mining and Technology, Xuzhou 221008, China
2 School of Resources and Geosciences, China University of Mining and Technology, Xuzhou 221116, China
3 China United Coalbed Methane Corporation, Ltd., Beijing 100011, China

Abstract Understanding the distribution of *in-situ* stresses is extremely important in a wide range of fields such as oil and gas exploration and development, CO_2 sequestration, borehole stability, and stress-related geohazards assessment. In the present study, the *in-situ* stress distribution in the Linxing area of eastern Ordos Basin, China, was analyzed based on well tested parameters. The maximum horizontal principal stress ($S_{H\max}$), minimum horizontal principal stress ($S_{h\min}$), and vertical stress (S_v) were calculated, and they were linearly correlated with burial depth. In general, two types of *in-situ* stress fields were determined in the Linxing area: (i) the *in-situ* stress state followed the relation $S_v > S_{H\max} > S_{h\min}$ in shallow layers with burial depths of less than about 940 m, indicating a normal faulting stress regime; (ii) the $S_{H\max}$ magnitude increased conspicuously and was greater than the S_v magnitude in deep layers with depths more than about 940 m, and the *in-situ* stress state followed the relation $S_{H\max} > S_v > S_{h\min}$, demonstrating a strike-slip faulting stress regime. The horizontal differential stress ($S_{H\max}$–$S_{h\min}$) increased with burial depth, indicating that wellbore instability may be a potentially significant problem when drilling deep vertical wells. The lateral stress coefficient ranged from 0.73 to 1.08 with an average of 0.93 in the Linxing area. The coalbed methane (CBM) reservoir permeability was also analyzed. No obvious exponential relationship was found between coal permeability and effective *in-situ* stress magnitude. Coal permeability was relatively high under a larger effective *in-situ* stress magnitude. Multiple factors, including fracture development, contribute to the variation of CBM reservoir permeability in the Linxing area of eastern Ordos Basin.

Received April 29, 2017; accepted August 20, 2017

E-mail: wju@cumt.edu.cn

Keywords *in-situ* stress, coalbed methane, permeability, lateral stress coefficient, Linxing area, Ordos Basin

1 Introduction

In general, the *in-situ* stress field and permeability are fundamental factors for coalbed methane (CBM) development (Zhao et al., 2016; Sun et al., 2017). *In-situ* stress is a type of internal stress in the Earth's crust, and it is greatly affected by tectonic a nd gravitational forces (Zoback et al., 2003; Kang et al., 2010; Zhou and Burbey, 2016). Knowledge of *in-situ* stress is significant in the fields of geologic science and engineering because it is essential to achieve a better understanding of phenomena related to oil and gas exploration and development (Finkbeiner et al., 2001; Bell, 2006; Tingay et al., 2009, 2010; Meng et al., 2011; Li et al., 2014; Ju and Sun, 2016; Ju et al., 2017), borehole stability (Zoback et al., 2003; Tingay et al., 2009; Nian et al., 2016; Rajabi et al., 2016; Ju et al., 2017), CO_2 sequestration (Bustin et al., 2008; Konstantinovskaya et al., 2012), reservoir management (Sibson, 1994; Binh et al., 2007; Nian et al., 2016), etc.

Coal seams serve as important reservoirs as they contain CBM adsorbed onto the inner surfaces. Estimation of *in-situ* stress for coal bearing strata has been applied widely in underground coal mines and CBM explorations within many coal basins (Bell and Bachu, 2003; Bell, 2006; Gentzis, 2009; Meng et al., 2011). Coal permeability is the dominant factor in CBM productivity, which is greatly influenced by the *in-situ* stress magnitude and orientation. Until now, it was generally accepted that, when other factors (e.g., fracture development; McKee et al., 1988; Ye et al., 1999) are equal, coal permeability decreases exponentially with increased effective stress magnitude (White et al., 2005; Bustin et al., 2008; Li et al., 2014).

Information of *in-situ* stress can facilitate the prediction of permeability and fluid flow in CBM reservoirs (Bell and Bachu, 2003; Bell, 2006). Therefore, an accurate understanding of the *in-situ* stress distribution is of immense importance for CBM reservoir permeability evaluation and recoverability assessment during CBM development (Meng et al., 2011; Paul and Chatterjee, 2011; Li et al., 2014; Zhao et al., 2016).

The Carboniferous and Permian sedimentary rocks in the Linxing area of eastern Ordos Basin host a significant volume of CBM resources in China (Guo et al., 2012). Insights into the *in-situ* stress state can effectively guide CBM exploration and development. Therefore, in this study, based on the well test parameters in the Linxing area, the *in-situ* stress distribution and types were first studied. Subsequently, the variation of coal permeability and the influencing factors were analyzed. The results can provide a reference for CBM accumulation and production in the Linxing area of eastern Ordos Basin.

2 Geological setting

The Ordos Basin is a typical intra-continental basin situated in central China. It extends over 2.5×10^5 km^2 (Ritts et al., 2004; Ju et al., 2015; Fig. 1). The Linxing area is economically significant and is located in the eastern Ordos Basin (Fig. 1), which is famous for widely distributed CBM resources (Guo et al., 2012). The tectonic structure is relatively stable and the stratigraphic strike is approximately NE-SW-trending with a westward dip of approximately 5°–10° (Yang, 2002; Ju et al., 2015).

In the Linxing area, the Carboniferous and Permian (mainly the Shanxi, Taiyuan, and Benxi Formations) sedimentary rocks contain a significant volume of CBM resources (Yang, 2002; Guo et al., 2012). The Benxi Formation (e.g., Well L-8, –1922.50 m to –1853.10 m), containing 1–4 coal seams, developed in a tidal flat-lagoon depositional system with a thickness of 51–70 m. The Taiyuan Formation (e.g., Well L-8, –1853.10 m to

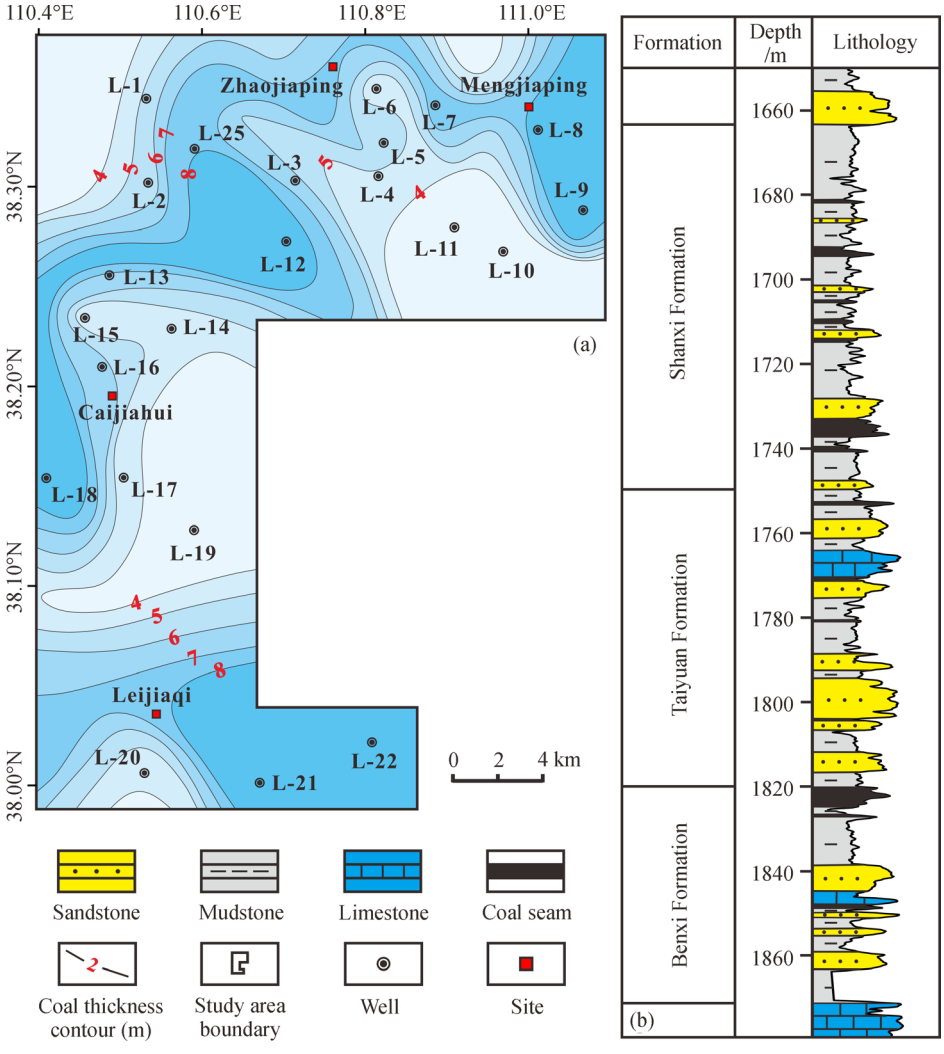

Fig. 1 Geologic conditions in the Linxing area of eastern Ordos Basin, China. (a) coal thickness in the Benxi Formation; (b) generalized stratigraphic column of the Benxi Formation, Taiyuan Formation and Shanxi Formation.

–1783.20 m) was predominantly deposited in a tidal flat and delta system, and its thickness ranges from 33 m to 76 m. The Shanxi Formation (e.g., Well L-8, –1783.20 m to –1678.00 m), containing 2–5 coal seams, was essentially deposited in a shallow water delta, lagoon-gulf sedimentary environment with a thickness of approximately 87–130 m (Gu et al., 2016; Zhao et al., 2016). These three large and well preserved coal-bearing formations in the Linxing area provide a good basis for CBM generation and accumulation (Guo et al., 2012; Zhao et al., 2016).

The commercial coal seams in the Linxing area are No. 4 + 5 coal seam of Shanxi Formation and No. 8 + 9 coal seam of Benxi Formation. The No. 4 + 5 coal seam is 0–8.8 m thick with an average thickness of 4.8 m. The No. 8 + 9 coal seam is 2.7–11.8 m thick with an average thickness of 7.1 m. The average vitrinite reflectance of the No. 4 + 5 and No. 8 + 9 coal seam varies primarily in the intervals of 0.75%–1.46% and 0.73%–1.50%, respectively, indicating that they are in the middle to late maturation stage, and can generate large amounts of hydrocarbons.

3 *In-situ* stress distribution

3.1 Methodology

The S_v, that is the lithostatic or overburden stress, is induced by the weight of overlying formations. The magnitude of S_v is usually assumed to be the most easily obtained component of the *in-situ* stress tensor because it can be calculated by integrating density logs (Eq. (1); Bell and Bachu, 2003; Meng et al., 2011; Rajabi et al., 2016).

$$S_v = \int_0^z \rho(z) g \mathrm{d}z, \tag{1}$$

where $\rho(z)$ is the density, z is depth and g is the acceleration due to gravity.

Previous studies (e.g., Brown and Hoek, 1978; Hoek and Brown, 1980; Meng et al., 2011) suggested that the magnitude of S_v can be accurately estimated by using Eq. (2):

$$S_v = 0.027z. \tag{2}$$

The $S_{h\min}$ is a key parameter in the designs of well drilling and reservoir stimulation. Several methods are available to determine the magnitude of $S_{h\min}$, and among them, the leak-off test (LOT) is an effective approach (Enever et al., 1996; White et al., 2002; Bell and Bachu, 2003; Zoback, 2007). In LOTs, the mud pressure in an open and isolated section of wellbore is increased to create a small tensile fracture (Zoback et al., 2003). In this study, extended leak-off tests (XLOTs), which can provide reliable information for calculating the magnitude of $S_{h\min}$, were conducted. XLOTs are longer and more comprehensive LOTs, wherein pumping is not stopped immediately after the leak-off pressure is observed. In addition, the fracture closure pressures (P_c) can be obtained through XLOTs (Enever et al., 1996; White et al., 2002; Brooke-Barnett et al., 2015; Rajabi et al., 2016).

Depending on the parameters obtained from the XLOTs, the magnitude of $S_{h\min}$, which is the magnitude of P_c at the test depth, can be determined (Eq. (3); White et al., 2002; Zoback et al., 2003).

$$S_{h\min} = P_c, \tag{3}$$

where P_c is the fracture closure pressure.

The $S_{H\max}$ magnitude is estimated based on additional information or assumptions (Zoback, 2007). For a vertical borehole and no fluid penetration in the formation, the magnitude of $S_{H\max}$ can be estimated based on Eq. (4) (Hubbert and Willis, 1957).

$$S_{H\max} = 3S_{H\min} - P_f - P_o + T, \tag{4}$$

where P_f is the recorded formation break-down pressure, P_o is the pore pressure, and T is the tensile strength of the rock.

All the parameters except for T can be obtained from the XLOT pressure records in Eq. (4). As the existing fractures retain no tensile strength during the second pressurizations, Bredehoeft et al. (1976) suggested that Eq. (4) can be simplified and rewritten as Eq. (5).

$$S_{H\max} = 3S_{H\min} - P_r - P_o, \tag{5}$$

where P_r is the reopening pressure at which closed fractures begin to reopen during repeated pressurizations.

In general, three types of *in-situ* stress regimes can be determined based on the relative magnitudes of $S_{H\max}$, $S_{h\min}$, and S_v (Anderson, 1951; Fig. 2):

(i) normal faulting stress regime: $S_v > S_{H\max} > S_{h\min}$;
(ii) strike-slip faulting stress regime: $S_{H\max} > S_v > S_{h\min}$;
(iii) reverse faulting stress regime: $S_{H\max} > S_{h\min} > S_v$.

3.2 Variation in the *in-situ* stress magnitudes with depth

The parameters of P_o, P_f, P_r, and P_c are important for calculating *in-situ* stress magnitudes. In the Linxing area, all these parameters increase linearly with burial depth (Fig. 3).

(i) pore pressure, ($R = 0.91$);
(ii) formation break-down pressure, ($R = 0.80$);
(iii) reopening pressure, ($R = 0.73$);
(iv) fracture closure pressure, ($R = 0.81$).

In the present study, based on 11 sets of parameters in the Linxing area, the magnitudes of S_v, $S_{H\max}$, and $S_{h\min}$ were calculated using Eqs. (2), (3), and (5) (Table 1), and further, they were both linearly correlated with burial depth (Fig. 4).

(i) $S_{H\max}$, ($R = 0.60$);
(ii) $S_{h\min}$, ($R = 0.81$).

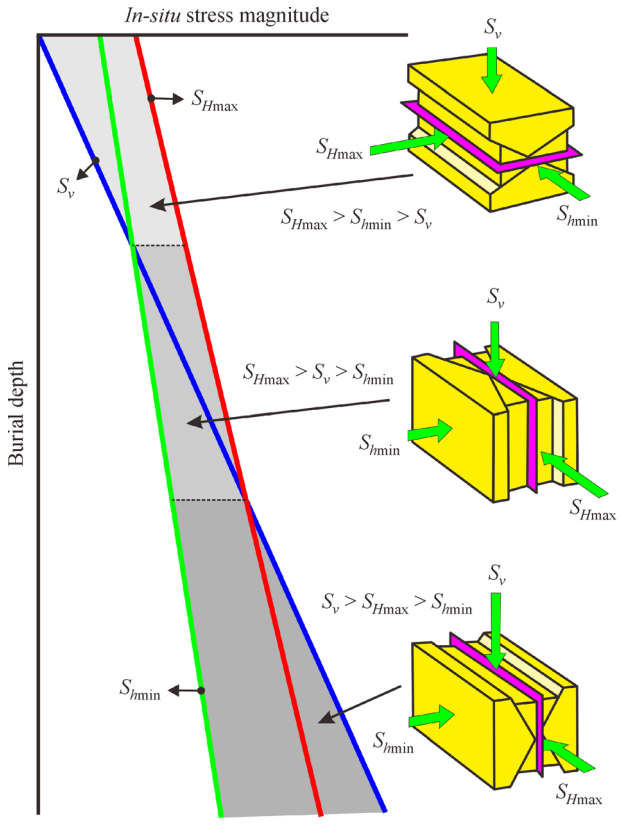

Fig. 2 Schematic illustration showing the Andersonian tectonic classification (after Brooke-Barnett et al., 2015). The pink plane represents the orientation of a propagated hydraulic fracture in the associated tectonic classification.

Generally, in sedimentary basins, the magnitude of $S_{h\min}$ is usually around 70% of the S_v magnitude (Meng et al., 2011). However, based on the calculation results (Fig. 4 (a)), the calculated $S_{h\min}$ may not accurately describe the actual $S_{h\min}$ magnitude and its variation in the Linxing area of eastern Ordos Basin.

In the Linxing area, the stress regime in the main coal-bearing strata was a strike-slip faulting regime ($S_{H\max} > S_v > S_{h\min}$; Fig. 4). Furthermore, the *in-situ* magnitude variation suggested that the stress regime followed the relation $S_v > S_{H\max} > S_{h\min}$ at depths less than approximately 940 m, indicating a normal faulting stress regime. In deep layers, the $S_{H\max}$ magnitude increased conspicuously and was greater than the S_v magnitude at depths more than approximately 940 m. The *in-situ* stress regime changed to $S_{H\max} > S_v > S_{h\min}$ in the deep layers, indicating a strike-slip faulting stress regime (Fig. 4(b)). The vertical transformation depth of the *in-situ* stress regime in the Linxing area was approximately 940 m (Fig. 4(b)).

The Zijinshan intrusive complex, situated at the east of Linxing area, formed mainly in 136.7–130.4 Ma of the Early Cretaceous (Chen et al., 2012). The rapid uplift-cooling process that occurred since 10 Ma at an average rate of 7°C/Ma caused changes in the subsurface structures. This resulted in the formation of many radial faults and variations in the burial depth of the overlying strata. As the S_v, $S_{H\max}$, and $S_{h\min}$ magnitude all increased linearly with burial depth, the *in-situ* stress distribution in regions near the Zijinshan intrusive complex also changed.

In addition, the relationship between the *in-situ* stress

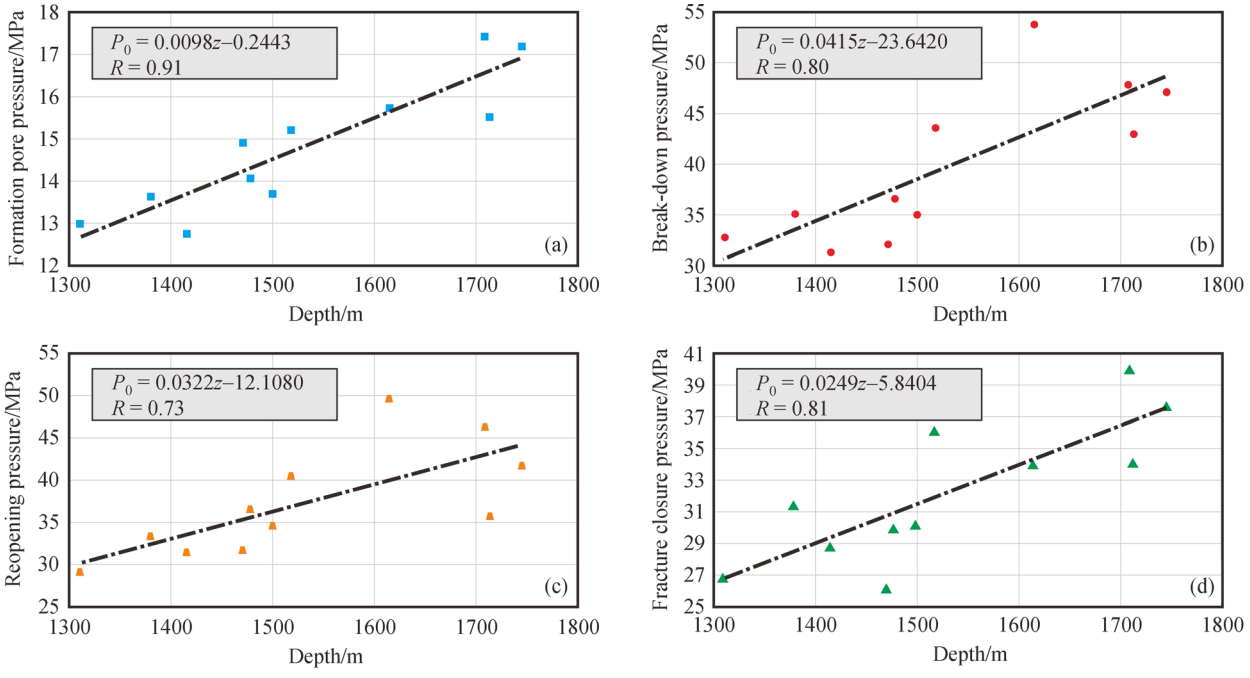

Fig. 3 Relationships among the P_o, P_f, P_r, and P_c and burial depth in the Linxing area. (a) Relationship between the P_o and burial depth, (b) relationship between the P_f and burial depth, (c) relationship between the P_r and burial depth, and (d) relationship between the P_c and burial depth.

Table 1 *In-situ* stress magnitudes in the Linxing area

Well	Test interval/(m, bgl)			P_o /(MPa)	P_f /(MPa)	P_r/ (MPa)	P_c /(MPa)	S_{Hmax} /(MPa)	S_{hmin} /(MPa)	S_v /(MPa)
	Top	Bottom	Average							
L-3	1411.30	1417.20	1414.25	12.75	31.33	31.30	28.71	42.08	28.71	38.18
	1495.90	1500.80	1498.35	13.68	35.08	34.61	30.12	42.07	30.12	40.46
L-4	1300.10	1317.40	1308.75	12.97	32.74	29.06	26.75	38.22	26.75	35.34
L-8	1466.60	1472.10	1469.30	14.90	32.04	31.70	26.05	31.55	26.05	39.67
L-12	1473.20	1480.10	1476.65	14.06	36.57	36.49	29.87	39.06	29.87	39.87
	1514.80	1519.20	1517.00	15.21	43.61	40.49	36.04	52.42	36.04	40.96
	1611.70	1616.70	1614.20	15.74	53.88	49.44	33.91	36.55	33.91	43.58
	1700.00	1717.00	1708.50	17.43	47.84	46.29	39.91	56.01	39.91	46.13
L-13	1737.80	1752.00	1744.90	17.20	47.08	41.74	37.63	53.96	37.63	47.11
L-16	1368.70	1387.80	1378.25	13.62	35.03	33.27	31.40	47.32	31.40	37.21
	1709.40	1715.50	1712.45	15.53	42.94	35.56	33.98	50.85	33.98	46.24

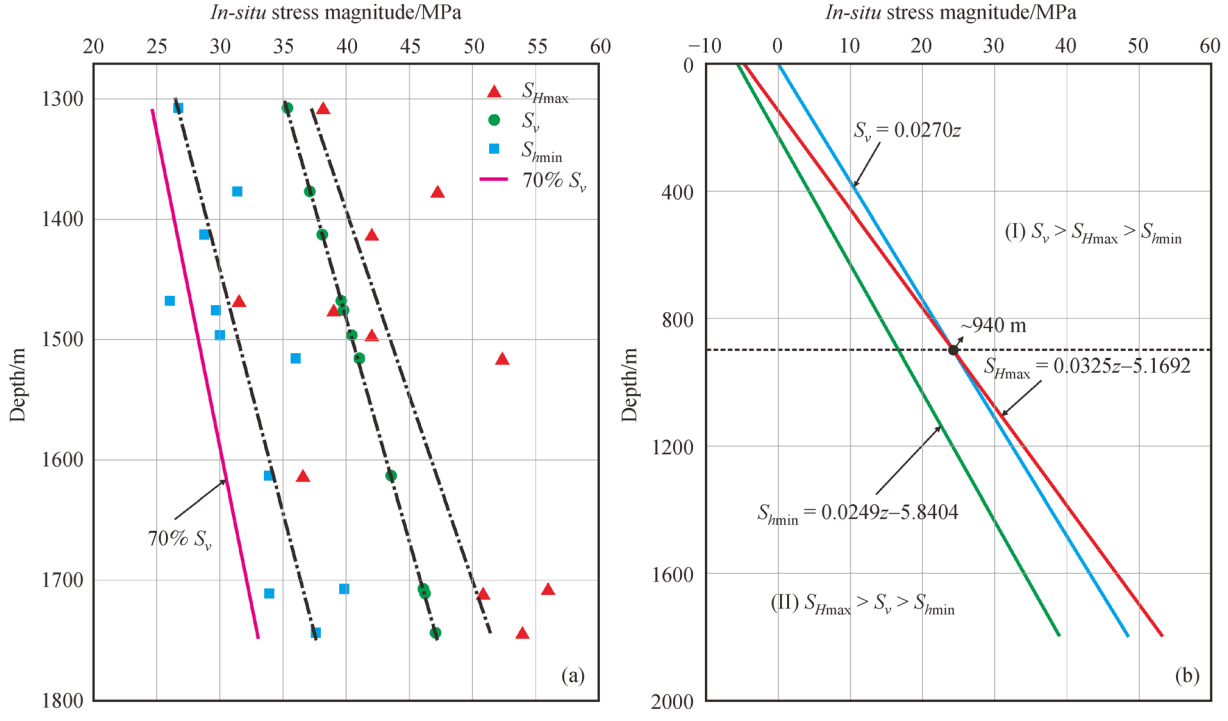

Fig. 4 The S_v, $S_{H\max}$, and $S_{h\min}$ magnitude in the Linxing area. (a) Distribution of calculated *in-situ* stress magnitudes, (b) distribution pattern of *in-situ* stress magnitudes.

magnitudes and burial depth also indicated that the horizontal differential stress ($S_{H\max}$–$S_{h\min}$) increased with burial depth (Fig. 4(b)). Therefore, for a vertical well, wellbore instability may be a potentially significant problem when drilling deep wells in the Linxing area because of the increasing ($S_{H\max}$–$S_{h\min}$) magnitude.

3.3 Stress ratio variation with burial depth

Generally, the lateral stress coefficient (λ) is defined and used to express the *in-situ* stress state at some point underground (Fig. 5; Brown and Hoek, 1978; Hoek and Brown, 1980; Meng et al., 2011; Yang et al., 2012). The coefficient is the ratio of the average horizontal stress magnitude (namely $S_{H\max}/2 + S_{h\min}/2$) to vertical stress magnitude (Eq. (6)):

$$\lambda = \frac{S_{H\max} + S_{H\min}}{2S_v}, \tag{6}$$

where λ is the lateral stress coefficient.

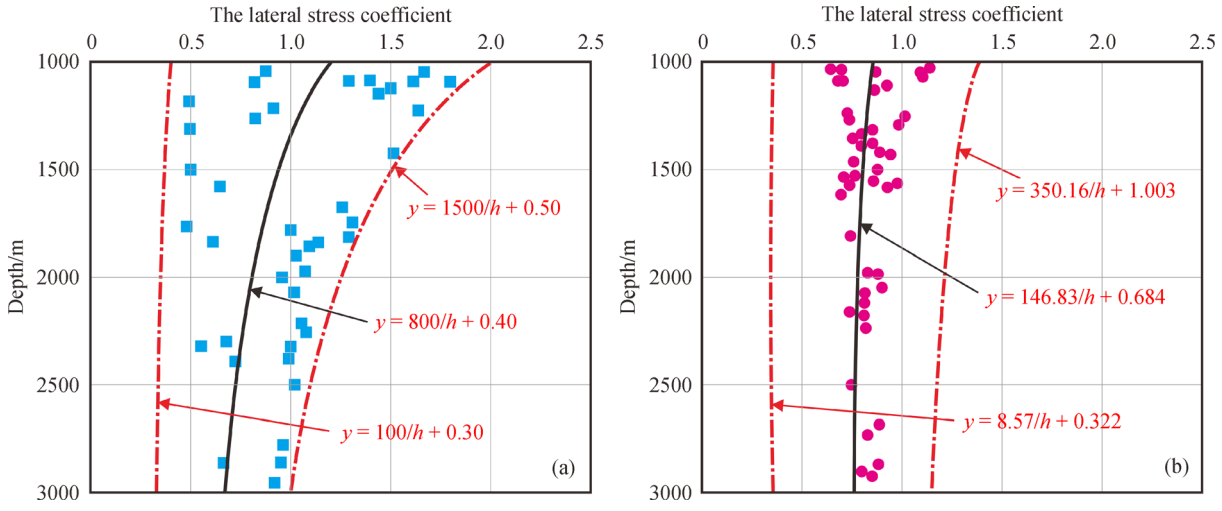

Fig. 5 Scatter diagrams showing lateral stress coefficient variation with burial depth (a) in the world (after Brown and Hoek, 1978; Hoek and Brown, 1980) and (b) in China (after Yang et al., 2012).

Brown and Hoek (1978) summarized the *in-situ* stresses worldwide (Fig. 5(a)) and found that the λ generally varied within limits defined by Eq. (7):

$$\frac{100}{h}+0.30\leqslant\lambda\leqslant\frac{1500}{h}+0.50. \tag{7}$$

Based on the expression of the inner and outer Hoek-Brown envelopes, λ can be rewritten in a general form (Eq. (8)) to reveal the linear relationship between λ and the reciprocal of burial depth.

$$\lambda=\frac{a}{h}+b, \tag{8}$$

where h is the burial depth, and a and b are coefficients.

Following Brown and Hoek's method, Yang et al. (2012) analyzed the *in-situ* distribution pattern in China (Fig. 5(b)) based on 3586 data values. The results indicated that λ in China generally varied within the limits defined by Eq. (9):

$$\frac{8.57}{h}+0.322\leqslant\lambda\leqslant\frac{350.16}{h}+1.003. \tag{9}$$

In the Linxing area, λ ranged from 0.73 to 1.08 with an average of 0.93 (Fig. 6). Obviously, all the values lie between the inner and outer Hoek-Brown *in-situ* stress envelopes representing the relationship between lateral stress coefficient and burial depth worldwide as well as in China (Fig. 6). The λ value also indicated that the *in-situ* stresses determined from the XLOTs were credible.

Furthermore, in the Linxing area, the ratio of $S_{H\max}/S_{h\min}$ ranged from 1.08 to 1.51 with an average of 1.38, the $S_v/S_{H\max}$ ratio varied between 0.78 and 1.26 with an average of 0.97, and the $S_v/S_{h\min}$ ratio changed in the interval of 1.14 and 1.52 with an average of 1.29 (Fig. 7). All the three stress ratios slowly decreased with burial depth (Fig. 7), suggesting that the horizontal stresses became dominant in deeper layers.

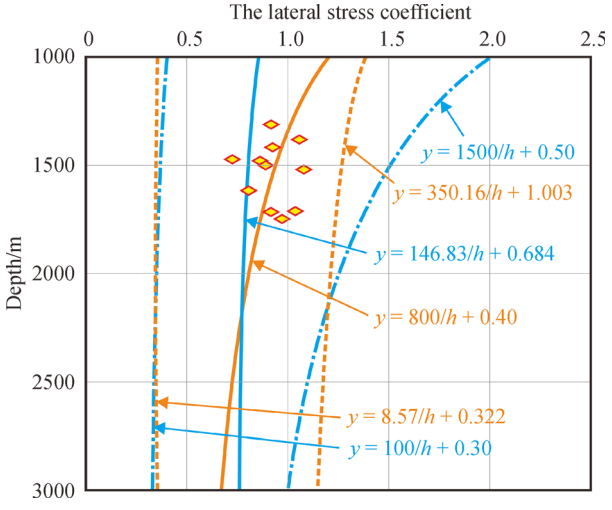

Fig. 6 The relationship between lateral stress coefficient and burial depth in the Linxing area.

Sun et al. (2017) indicated that the tectonic stress intensity controlled the vertical transformation of *in-situ* stress types. The CBM basins in China experienced strong tectonic stress because of the effects of plate tectonics. However, owing to the differences in the tectonic stress intensity in different basins or in different parts of the same basin, various *in-situ* stress types were induced for different burial depths and different *in-situ* stress vertical transformation depths. For example, the vertical transformation depth is approximately 600–700 m in the southern Qinshui Basin (Meng et al., 2011) and approximately 700–1000 m in the eastern margin of Ordos Basin (Zhao et al., 2016).

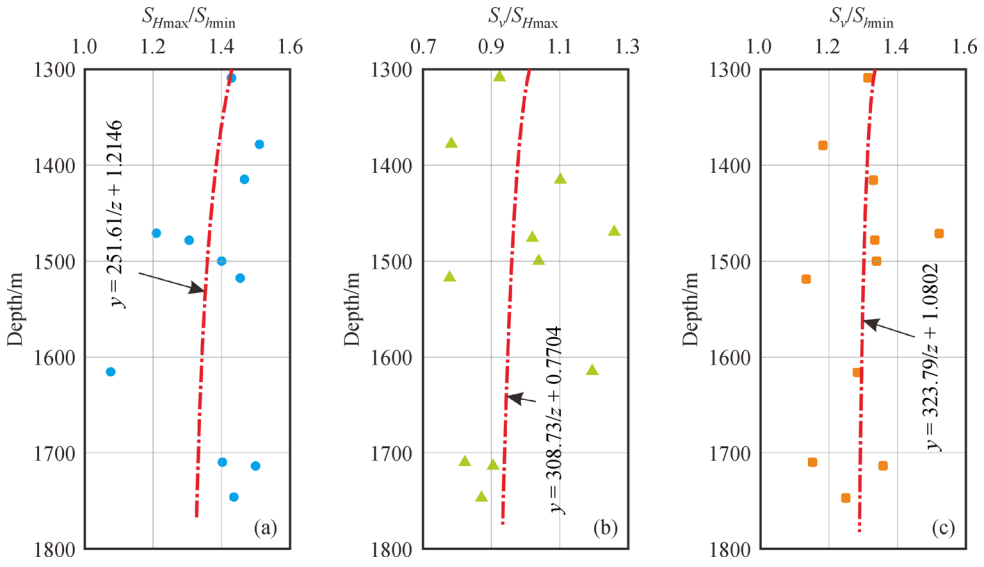

Fig. 7 Scatter diagrams showing the relationship between *in-situ* stress ratio and burial depth in the Linxing area. (a) Relationship between the $S_{H\max}/S_{h\min}$ ratio and burial depth, (b) relationship between the $S_v/S_{H\max}$ ratio and burial depth, and (c) relationship between the $S_v/S_{h\min}$ ratio and burial depth.

3.4 Pore pressure/stress coupling

Pore pressure is an important component of the stress tensor, which is necessary for calculating stress magnitudes and effective stresses. Generally, the spatial-temporal changes in the components of the stress tensor (ΔS) are a function of changes in pore pressure (ΔP_0), and this behavior is termed "pore pressure/stress coupling ($\Delta S/\Delta P_0$)" (Hillis, 2001; Tingay et al., 2009).

The $S_{h\min}$ is a primary controlling factor for the fracture gradient and a major constant on the propagation of hydraulic fractures (Meng et al., 2011), which is dependent upon pore pressure. For example, Altmann et al. (2010) reported that change in $S_{h\min}$ magnitude was on average approximately 64% of the change in pore pressure according to worldwide measurement data.

Based on the theory of Matthews and Kelly (1967), the relationship between effective $S_{h\min}$ and effective S_v follows Eq. (10):

$$S_{h\min} = K_0(S_v - P_0) + P_0, \tag{10}$$

where K_0 is the effective stress ratio.

In the Linxing area, this relationship (Fig. (8)) is expressed as shown in Eq. (11). This equation indicates a relationship between the effective stresses similar to that in other sedimentary basins or areas (e.g., the southern Qinshui Basin; Meng et al., 2011).

$$S_{h\min} = 0.7708(S_v - P_0) + P_0. \tag{11}$$

In the Linxing area, the effective stress ratio is 0.7708, which is lower than the commonly used value (K_0= 0.80) in shales in deep petroleum basins (Zhang et al., 2008), and larger than the values (K_0= 0.505–0.540) in coal seams of southern Qinshui Basin (Meng et al., 2011).

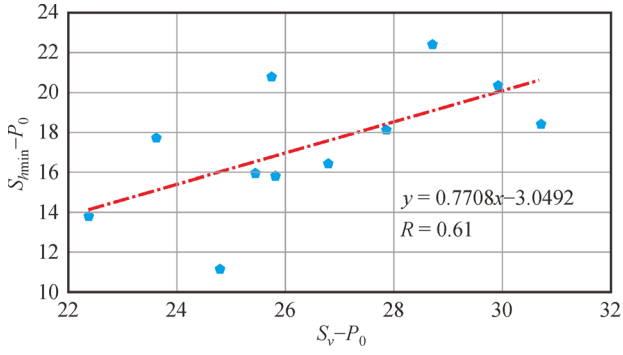

Fig. 8 The relationship between effective $S_{h\min}$ and effective S_v in the Linxing area.

In addition, Zoback et al. (2003) stated that as the Earth's crust contains widely distributed faults, fractures, and planar discontinuities at different scales and with different orientations, the ratio of effective $S_{H\max}$ (σ_1, $\sigma_1 \equiv S_{H\max}-P_0$) and effective $S_{h\min}$ (σ_3, $\sigma_3 \equiv S_{h\min}-P_0$) cannot exceed the frictional strength of planar discontinuities.

4 CBM reservoir permeability

4.1 Variation in coal permeability

In the present study, 14 coal pillars (length approximately 5.00 cm, diameter approximately 2.45 cm) obtained from No. 4 + 5 and No. 8 + 9 coal seams in the Linxing area were prepared for permeability tests. The permeability was

measured based on the unsteady pressure drop method (Jones, 1972). The experimental results indicated that, in the Linxing area, the permeability in No. 4 + 5 coal seam varied between 0.036 mD and 9.620 mD with an average of 1.999 Md, and that in No. 8 + 9 coal seam ranged between 0.080 mD and 9.860 mD with an average of 2.310 mD (Table 2).

4.2 Factors affecting coal permeability

Permeability is an important parameter for CBM reservoirs. The *in-situ* stresses control the variation in permeability by causing changes in pore structures, variations in the fracture density, and orientation of coal seams (Zhao, 1997). Under identical conditions, Somerton et al. (1975) and Seidle et al. (1992) revealed an exponential relationship between coal permeability and the magnitude of *in-situ* stress by performing regression analysis. It was found that, generally, coal permeability declines exponentially with an increase in the effective stress magnitude (White et al., 2005; Bustin et al., 2008; Li et al., 2014).

However, in the Linxing area, the results as presented in Table 2 indicate that coal permeability does not decline exponentially with increased effective *in-situ* stress magnitude. On the contrary, the permeability is relatively higher for larger stress magnitudes (Table 2). Therefore, the results indicate that coal permeability in the Linxing area is affected by many factors, such as the fracture development and orientation, petrographic constituents, pore structures, and engineering operations (Ye et al., 1999; Zhang et al., 2007; Li et al., 2014).

In the present study, the fractures in coal seams were considered to understand the variation in coal permeability. Sample A (depth: –1823.00 m) and sample B (–1827.10 m) were both obtained from the No. 8 + 9 coal seam in Well L-4 in the Linxing area. These two samples have mostly similar parameters, such as burial depth and the *in-situ* stress magnitude. However, sample B developed more fractures (fracture density: 6.0/cm) than sample A (fracture density: 1.2/cm), and the majority of these fractures were not filled with materials (Fig. 9). Correspondingly, sample B had a relatively larger coal permeability of 9.860 mD, compared with 0.080 mD for sample A. The results indicated that the development of fractures combined with the degree of filling for fractures in coal seams may have an important or even a dominant controlling effect on the permeability in the Linxing area.

In addition, in this study, coal permeability was measured in the laboratory instead of *in-situ*, which may also be the reason for the current non-stress-dependent permeability distribution pattern obtained in the Linxing area.

Table 2 Coal permeability and effective *in-situ* stress magnitudes in the Linxing area

Coal seam	Number of measured coal plugs	Depth /(m)		Permeability /(mD)		Effective					
						$S_{H\max}$/(MPa)		$S_{h\min}$/(MPa)		S_v/(MPa)	
		Min–Max	Average	Min–Max	Average	Min–Max	Average	Min–Max	Average	Min–Max	Average
No. 4 + 5	7	1635.00–1886.90	1723.60	0.036–9.620	1.999	32.190–37.908	34.201	19.092–22.896	20.430	28.366–32.699	29.890
No. 8 + 9	7	1769.20–1930.20	1831.89	0.080–9.860	2.310	35.236–38.891	36.659	21.079–23.550	22.065	30.675–33.444	31.753

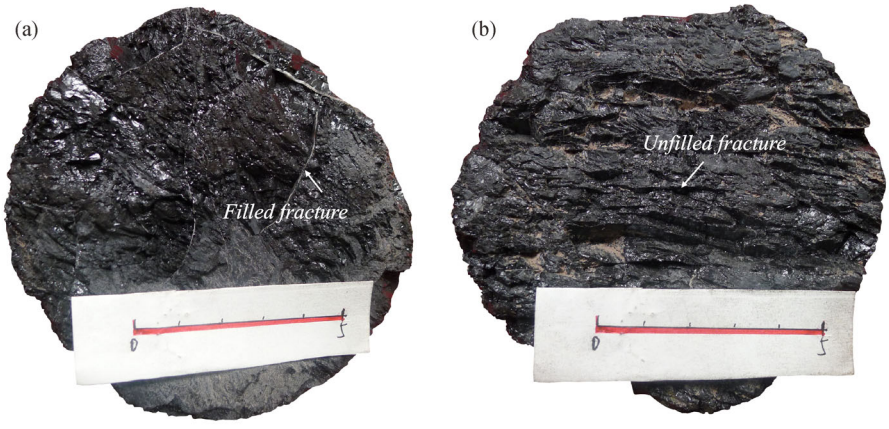

Fig. 9 Photos showing the development of fractures in coal seams in the Linxing area. (a) Well L-4, No. 8 + 9 coal seam, –1823.00 m; (b) Well L-4, No. 8 + 9 coal seam, –1827.10 m.

5 Conclusions

Knowledge of *in-situ* stresses is useful in a varity of fields, such as hydrocarbon exploration and development, and for the purposes such as examination of borehole stability and stress-related geohazards assessment. In the present study, the *in-situ* stress distribution and CBM reservoir permeability in the Linxing area, eastern Ordos Basin, China, were studied and analyzed.

1) The distribution patterns of the $S_{H\max}$, $S_{h\min}$ and S_v magnitude with burial depth were obtained. The results indicated that all three parameters were linearly correlated with burial depth. The linear correlations can be expressed as follows: $S_{H\max}=0.0325z-5.1692$, $S_{h\min}=0.0249z-5.8404$, and $S_v=0.027z$. In addition, the horizontal differential stress ($S_{H\max}-S_{h\min}$) magnitude increased with burial depth, suggesting that wellbore instability may be a potentially significant problem when drilling deep vertical wells in the Linxing area.

2) In the Linxing area, the presence of two types of *in-situ* stress fields was determined: (i) in shallow layers with depths less than approximately 940 m, and the *in-situ* stress state followed the relation $S_v > S_{H\max} > S_{h\min}$, indicating a normal faulting stress regime; (ii) in deep layers with depths more than approximately 940 m, and the *in-situ* stress state followed the relation $S_{H\max} > S_v > S_{h\min}$, indicating a strike-slip faulting stress regime. The vertical transformation depth of the *in-situ* stress regime in the Linxing area was approximately 940 m.

3) The lateral stress coefficient in the Linxing area ranged from 0.73 to 1.08 with an average of 0.93.

4) No obvious exponential relationships were found between coal permeability and *in-situ* stress magnitude. Fractures in coal seams may have an important or even a dominant effect on the permeability in the Linxing area.

Acknowledgements We would like to express our gratitude to the reviewers for offering constructive suggestions and comments which improved this manuscript in many aspects. This work was supported by the National Science and Technology Major Project (No. 2016ZX05066), the National Natural Science Foundation of China (Grant Nos. 41702130, 41672149, and 41672146), the Fundamental Research Funds for the Central Universities (2015XKZD07), and Priority Academic Program Development of Jiangsu Higher Education Institutions (PAPD).

References

Altmann J B, Muller T M, Muller B I R, Tingay M R P, Heidbach O (2010). Poroelastic contribution to the reservoir stress path. Int J Rock Mech Min Sci, 47(7): 1104–1113

Anderson E M (1951). The Dynamics of Faulting and Dyke Formation with Applications to Britain (2nd ed). Edinburgh: Oliver

Bell J S (2006). *In-situ* stress and coal bed methane potential in Western Canada. Bull Can Pet Geol, 54(3): 197–220

Bell J S, Bachu S (2003). *In situ* stress magnitude and orientation estimates for Cretaceous coal-bearing strata beneath the plains area of central and southern Alberta. Bull Can Pet Geol, 51(1): 1–28

Binh N T T, Tokunaga T, Son H P, Van Binh M (2007). Present-day stress and pore pressure fields in the Cuu Long and Nam Con Son Basins, offshore Vietnam. Mar Pet Geol, 24(10): 607–615

Bredehoeft J D, Wolff R G, Keys W S, Shuter E (1976). Hydraulic fracturing to determine regional *in situ* stress field, Piceance Basin, Colorado. Geol Soc Am Bull, 87(2): 250–258

Brooke-Barnett S, Flottmann T, Paul P K, Busetti S, Hennings P, Reid R, Rosenbaum G (2015). Influence of basement structures on *in situ* stresses over the Surat Basin, southeast Queensland. J Geophys Res Solid Earth, 120(7): 4946–4965

Brown E T, Hoek E (1978). Trends in relationships between measured *in situ* stresses and depth. Int J Rock Mech Min Sci Geomech Abstr, 15 (4): 211–215

Bustin R M, Cui X, Chikatamarla L (2008). Impacts of volumetric strain on CO_2 sequestration in coals and enhanced CH_4 recovery. Am Assoc Pet Geol Bull, 92: 15–29

Chen G, Ding C, Xu L M, Zhang H R, Hu Y X, Yang F, Li N, Mao X N (2012). Analysis on the thermal history and uplift process of Zijinshan intrusive complex in the eastern Ordos Basin. Chin J Geophys, 55(11): 3731–3741 (in Chinese)

Enever J R, Yassir N, Willoughby D R, Addis M A (1996). Recent experience with extended leak-off tests for *in-situ* stress measurement in Australia. The APPEA Journal, 36(1): 528–535

Finkbeiner T, Zoback M, Flemings P, Stump B (2001). Stress, pore pressure, and dynamically constrained hydrocarbon columns in the South Eugene Island 330 field, northern Gulf of Mexico. Am Assoc Pet Geol Bull, 85: 1007–1031

Gentzis T (2009). Stability analysis of horizontal coalbed methane well in the Rocky Mountain Front Ranges of southeast British Columbia, Canada. Int J Coal Geol, 77(3–4): 328–337

Gu J Y, Zhang B, Guo M Q (2016). Deep coalbed methane enrichment rules and its exploration and development prospect in Linxing block. Journal of China Coal Society, 41(1): 72–79 (in Chinese)

Guo B G, Xu H, Meng S Z, Zhang W Z, Liu Y N, Luo H H, Li Y, Shen W M (2012). Geology condition analysis for unconventional gas co-exploration and concurrent production in Linxing area. China Coalbed Methane, 9(4): 3–6 (in Chinese)

Hillis R R (2001). Coupled changes in pore pressure and stress in oil fields and sedimentary basins. Petrol Geosci, 7(4): 419–425

Hoek E, Brown E T(1980). Underground Excavations in Rock. London: The Institution of Mining and Metallurgy

Hubbert M K, Willis D G (1957). Mechanics of hydraulic fracturing. Petroleum Transactions, the American Institute of Mining. Metallurgical, and Petroleum Engineers, 210: 153–168

Jones S C (1972). A rapid accurate unsteady-state klinkenberg permeameter. Society of Petroleum Engineers Journal, 12(5): 383–397

Ju W, Shen J, Qin Y, Meng S Z, Wu C F, Shen Y L, Yang Z B, Li G Z, Li C (2017). *In-situ* stress state in the Linxing region, eastern Ordos Basin, China: implications for unconventional gas exploration and production. Mar Pet Geol, 86: 66–78

Ju W, Sun W F (2016). Tectonic fractures in the Lower Cretaceous Xiagou Formation of Qingxi Oilfield, Jiuxi Basin, NW China. Part two: numerical simulation of tectonic stress field and prediction of tectonic fractures. J Petrol Sci Eng, 146: 626–636

Ju W, Sun W F, Hou G T (2015). Insights into the tectonic fractures in the Yanchang Formation interbedded sandstone-mudstone of the Ordos Basin based on core data and geomechanical models. Acta Geol Sin, 89(6): 1986–1997

Kang H, Zhang X, Si L, Wu Y, Gao F (2010). *In-situ* stress measurements and stress distribution characteristics in underground coal mines in China. Eng Geol, 116(3–4): 333–345

Konstantinovskaya E, Malo M, Castillo D A (2012). Present-day stress analysis of the St. Lawrence Lowlands sedimentary basin (Canada) and implications for caprock integrity during CO_2 injection operations. Tectonophysics, 518: 119–137

Li Y, Tang D Z, Xu H, Yu T X (2014). *In-situ* stress distribution and its implication on coalbed methane development in Liulin area, eastern Ordos Basin, China. J Petrol Sci Eng, 122: 488–496

Matthews W R, Kelly J (1967). How to predict formation pressure and fracture gradient. Oil Gas J, 65: 92–106

McKee C R, Bumb A C, Koenig R A (1988). Stress-dependent permeability and porosity of coal and other geologic formations. Society of Petroleum Engineers Journal, 3(1): 81–91

Meng Z P, Zhang J C, Wang R (2011). *In-situ* stress, pore pressure and stress-dependent permeability in the Southern Qinshui Basin. Int J Rock Mech Min Sci, 48(1): 122–131

Nian T, Wang G W, Xiao C W, Zhou L, Deng L, Li R J (2016). The *in situ* stress determination from borehole image logs in the Kuqa Depression. J Nat Gas Sci Eng, 34: 1077–1084

Paul S, Chatterjee R (2011). Determination of *in situ* stress direction from cleat orientation mapping for coal bed methane exploration in south-eastern part of Jharia coalfield, India. Int J Coal Geol, 87(2): 87–96

Rajabi M, Tingay M R P, Heidbach O (2016). The present-day state of tectonic stress in the Darling Basin, Australia: implications for exploration and production. Mar Pet Geol, 77: 776–790

Ritts B D, Hanson A D, Darby B J, Nanson L, Berry A (2004). Sedimentary record of Triassic intraplate extension in North China: evidence from the nonmarine NW Ordos Basin, Helan Shan and Zhuozi Shan. Tectonophysics, 386(3–4): 177–202

Seidle J P, Jeansonne M W, Erickson D J (1992). Application of matchstick geometry to stress dependent permeability in coals. In: SPE Rocky Mountain Regional Meeting. Society of Petroleum Engineers, Casper.

Sibson R (1994). Crustal stress, faulting and fluid flow. In: Parnell J, ed. Geofluids: Origin, Migration and Evolution of Fluids in Sedimentary Basins. Geological Society of London, Special Publication 78: 69–84

Somerton W H, Soylemezoglu I M, Dudley R C (1975). Effect of stress on permeability of coal. Int J Rock Mech Min Sci, 12(5–6): 129–145

Sun L Z, Kang Y S, Wang J, Jiang S Y, Zhang B, Gu J Y, Ye J P, Zhang S R(2017). Vertical transformation of *in-situ* stress types and its control on coalbed reservoir permeability. Geological Journal of China Universities, 23(1): 148–156 (in Chinese)

Tingay M R P, Hills R R, Morley C K, King R C, Swarbrick R E, Damit A R (2009). Present-day stress and neotectonics of Brunei: implications for petroleum exploration and production. Am Assoc Pet Geol Bull, 93(1): 75–100

Tingay M R P, Morley C K, Hillis R R, Meyer J (2010). Present-day stress orientation in Thailand's basins. J Struct Geol, 32(2): 235–248

White A J, Traugott M O, Swarbrick R E (2002). The use of leak-off tests as means of predicting minimum *in-situ* stress. Petrol Geosci, 8(2): 189–193

White C M, Smith D H, Jones K L, Goodman A L, Jikich S A, LaCount R B, DuBose S B, Ozdemir E, Morsi B I, Schroeder K T (2005). Sequestration of carbon dioxide in coal with enhanced coalbed methane recovery: a review. Energy Fuels, 19(3): 659–724

Yang J J (2002). Tectonic Evolution and Oil-gas Reservoirs Distribution in Ordos Basin. Beijing: Petroleum Industry Press (in Chinese)

Yang S X, Yao R, Cui X F, Chen Q C, Huang L Z (2012). Analysis of the characteristics of measured stress in Chinese mainland and its active blocks and North-South seismic belt. Chin J Geophys, 55(12): 4207–4217 (in Chinese)

Ye J P, Shi B S, Zhang C C (1999). Coal reservoir permeability and its controlled factors in China. Journal of China Coal Society, 24(2): 118–122 (in Chinese)

Zhang J, Standifird W B, Lenamond C (2008). Casing ultradeep, ultralong salt sections in deep water: a case study for failure diagnosis and risk mitigation in record-depth well. Society of Petroleum Engineers, 114273

Zhang J, Standifird W B, Roegiers J C, Zhang Y (2007). Stress-dependent permeability in fractured media: from lab experiments to engineering applications. Rock Mech Rock Eng, 40(1): 3–21

Zhao J L, Tang D Z, Xu H, Li Y, Li S, Tao S, Lin W J, Liu Z X (2016). Characteristic of *in situ* stress and its control on the coalbed methane reservoir permeability in the eastern margin of the Ordos Basin, China. Rock Mech Rock Eng, 49(8): 3307–3322

Zhao Q B (1997). Potential evaluation parameters and exploration direction in a coalbed gas region. Petroleum Exploration and Development, 24(1): 6–10 (in Chinese)

Zhou X J, Burbey T J (2016). The mechanism of faulting regimes change over depths in the sedimentary layers in an intracratonic basin. Arab J Geosci, 9(1): 1–11

Zoback M D (2007). Reservoir Geomechanics. Cambridge: Cambridge University Press

Zoback M D, Barton C A, Brudy M, Castillo D A, Finkbeiner T, Grollimund B R, Moos D B, Peska P, Ward C D, Wiprut D J (2003). Determination of stress orientation and magnitude in deep wells. Int J Rock Mech Min Sci, 40(7–8): 1049–1076